

Boundary layer turbulence in transitional and developed states

By J. M. Wallace[†], G. I. Park, X. Wu[‡] AND P. Moin

Using the recent DNS by Wu and Moin (2010) of a flat-plate boundary layer with a passively heated wall, statistics of the turbulence in transition at $Re_\theta = 500$ where spots merge (distributions of the mean velocity, rms velocity and vorticity component fluctuations, kinetic energy production and dissipation rates and enstrophy) have been compared to these statistics for the developed boundary layer turbulence at $Re_\theta = 1850$. When the distributions in the transitional region, determined in narrow planes $0.03Re_\theta$ wide, exclude regions and times when the flow is not turbulent, they closely resemble the distributions in the developed turbulent state at the higher Reynolds number, especially in the buffer and sublayers. The skin friction coefficient, determined in this conditional manner in the transitional flow is, of course, much larger than that obtained by including both turbulent and non-turbulent information there, and is consistent with a value obtained by extrapolating from the developed turbulent region. Individual hairpin vortices have been identified using vorticity lines in the transitional and developed turbulence, and they have quite similar characteristics in both cases. Some of these vortices appear to emerge out of sheets of unorganized vorticity in the viscous sublayer. Hairpin vortices are closely associated with the processes that transport momentum and heat within the boundary layer. An octant analysis based on the combinations of signs of the velocity and temperature fluctuations, u , v and θ , shows that this transport is predominantly of the mean gradient type over much of both the transitional and developed flows. The results add strong evidence to the view that there is little difference between the structure and transport processes of a developed turbulent boundary layer and of turbulent spots that appear in transition.

1. Introduction

Flows near bounding solid surfaces have been extensively studied since the landmark paper of Prandtl (1904), over a century ago, in which he formulated the governing boundary layer equations as simplifications of the general equations of fluid motion. Boundary layers occur in a large number of natural and technological settings, e.g. the earth's atmosphere, on the surfaces of land, sea and air vehicles, and in the human body's conduits among many others, so they are obviously of great scientific, engineering and even medical importance. Such flows transition from a laminar to a turbulent state when the Reynolds number is sufficiently large. The transition routes to turbulence can vary and depend on several factors, including the intensity of turbulence in the free-stream flow above the initial laminar boundary layer. Regardless of the route, eventually small, individual islands of turbulence develop, called turbulent spots, which were first visualized and described by Emmons (1951). These spots grow as they convect downstream until they merge into one another and the whole boundary layer becomes completely turbulent.

[†] Burgers Program for Fluid Dynamics, University of Maryland

[‡] Department of Mechanical Engineering, Royal Military College of Canada

A great deal of experimental research, initiated as early as fifty years ago and continued in the three decades thereafter, was carried out in an attempt to characterize and understand the dynamics of turbulent spots. Representative of this is the investigation of Cantwell *et al.* (1978). These studies were motivated by the idea that turbulent spots are turbulent boundary layers in formation, albeit in a less complex state than when the turbulence becomes developed. By generating spots in Blasius boundary layers with controllable disturbances of sufficient amplitude and employing phase averaging, many details about their structure were deduced (e.g. Wygnanski *et al.* 1979 and Katz *et al.* 1990).

By contrast, even though direct numerical simulations (DNS) of turbulent shear flows have been possible for about twenty-five years, turbulent spots have not received nearly so much attention by this means. Henningson *et al.* (1987) investigated turbulent spots in both plane channel and boundary layer flow simulations. Later, Henningson & Kim (1991) extensively analysed the channel flow case, including mean and rms velocity component distributions determined from data extracted from the turbulent cores of the spots compared with distributions in fully developed channel flow. Singer & Joslin (1994) and Singer (1996) created a turbulent spot simulation in a flat-plate laminar boundary layer by a localized injection of fluid at the wall. This mimicked one of the experimental means of generating controllable spots that begins with a hairpin vortex. They followed the development of the hairpin vortex as it evolved into a turbulent spot and examined its characteristics. Jacobs & Durbin (2001) simulated by-pass transition of a boundary layer, perturbed by free-stream turbulence, in which spots appear, merge and evolve into a developed turbulent state. Krishnan & Sandham (2006) carried out a DNS to study the interaction of turbulent spots in a supersonic boundary layer at Mach 2. The spots develop because of localized blowing at the wall into an otherwise laminar flow. The simulations of single spots and the merging of two spots both show the spot structure to be dominated by many well-formed hairpin vortices when visualized with iso-surfaces of the second invariant of the velocity gradient tensor, $Q \equiv -1/2\partial U_i/\partial x_j\partial U_j/\partial x_i$.

There is a vast literature on developed turbulent boundary layers. The most authoritative early experiment documenting some of the statistical properties of the velocity field was that of Klebanoff (1954), which included the turbulent kinetic energy budget with the dissipation rate roughly estimated. Purtell, with Klebanoff and Buckley (1981), later examined the question of when a boundary layer reaches a self-similar fully developed turbulent state. Using a multi-sensor hot-wire probe that could simultaneously measure the velocity vector and velocity gradient tensor components, Balint *et al.* (1992) documented the small-scale turbulent boundary layer properties, vorticity and dissipation rate, and compared their experimental values to those from the first DNS of a turbulent boundary layer, which was carried out by Spalart (1988).

In spite of little supporting experimental evidence, Theodorsen (1952) hypothesized that the underlying structure of boundary layers was made up of vortex loops of superimposed scales, in the form of “horseshoes”. However, this hypothesis was little noted, and there was not much interest in the structure of bounded flows until the visualization experiments of Kline *et al.* (1967) in a turbulent boundary layer and Corino & Brodkey (1969) in a turbulent pipe flow.

These visualizations sparked a great deal of interest and effort to try to characterize and understand the dynamical importance of coherent structures in bounded flows. One of the first of these efforts was the turbulent channel flow quadrant analysis that Wallace *et al.* (1972) conceptualized and carried out in order to quantify the contributions to the

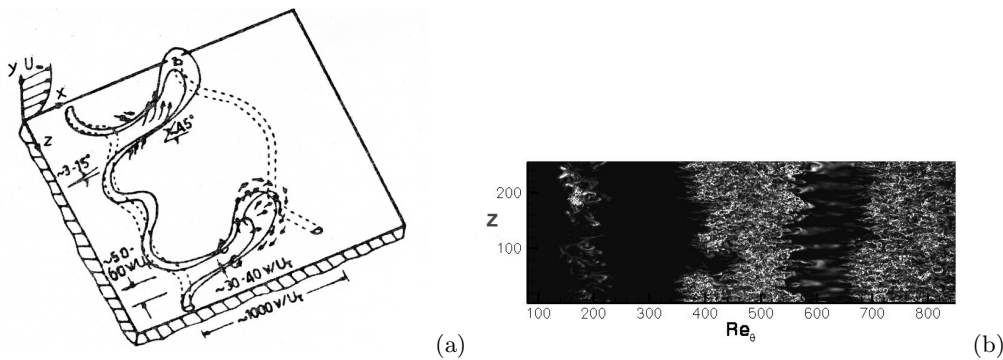


FIGURE 1. (a) Conceptual sketch of vortices in wall bounded flows, Wallace (1982). (b) Example of merged turbulent spots in the vicinity of $Re_\theta \approx 500$ marked by isosurfaces of enstrophy.

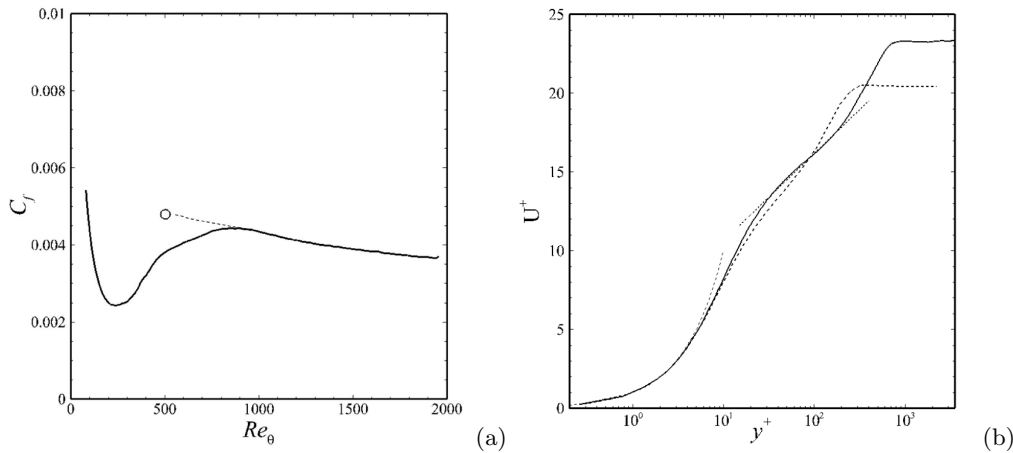


FIGURE 2. (a) Coefficient of friction as a function of Re_θ . Solid line, Wu and Moin (2010); open circle, data obtained in merged turbulent spots. (b) Mean streamwise velocity distribution: solid, $Re_\theta = 1850$; dashed, $Re_\theta = 500$; dash-dot, $U^+ = y^+$ near the wall and $U^+ = 2.41 \ln y^+ + 5.7$ in the logarithmic layer.

Reynolds shear stress of the ejection and sweep motions visualized by Corino & Brodkey.

Willmarth (1975) reviewed much of the work up until this point. Wallace (1982) attempted to pull together most of the then existing experimental evidence about the vortices that he and others thought were the underlying structure of bounded flows and that were the dynamical engine producing most of the Reynolds shear stress. His sketch of these conceptualized structures is shown in Fig. 1(a). A few years later Wallace (1985) added to this experimental evidence, and also included evidence from vortex element and large-eddy simulations that had become available. In their investigation of the structure of the vorticity field in their LES of turbulent channel flow, Moin & Kim (1985) used vorticity lines, integrated through the flow from judiciously chosen starting locations, to demonstrate that hairpin vortices are prominent in turbulent channel flow. In the appendix of a followup study, Kim & Moin (1986) showed that this is also true when all the scales were well resolved in a DNS. However, vorticity lines began to fall into disfavor because, as often pointed out and reiterated by Robinson (1991), they are field lines that can be drawn wherever the flow is rotational, regardless of whether or not a true vortex

exists in a part of the field. Only when the vorticity lines occur in bundles, spatially coherent in comparison to the more disorganized vorticity lines in their vicinity, do they appear to indicate vortices. On the other hand, a virtue that such lines have is that the vortical structures they can reveal do not depend on setting a detection threshold, unlike all the vortex identifiers based on the velocity gradient tensor or based on a low pressure criterion. Furthermore, vorticity lines can be used to isolate a single vortical structure.

Adrian (2007) and his group observed from planar PIV and DNS that hairpin vortices occur in packets and that existing hairpins can spawn new ones. The recent DNS of a turbulent boundary layer by Wu & Moin (2009), in which the flow was allowed to spatially develop from a Blasius boundary layer into a turbulent one, showed a forest of hairpins when visualized with the Q criterion, although the Reynolds number reached, $Re_\theta \approx 900$, was still low. This simulation has created a lot of interest and some controversy, because well-formed, post-transition hairpins had never been observed in such abundance in bounded flow DNS before. It has been suggested that the hairpins visualized in this simulation are merely the remnants of transition and that they do not survive when the boundary layer is fully turbulent. This contention appears to be supported by the boundary layer DNS of Schlatter *et al.* (2010) at Re_θ up to 4,300 in which hairpins were not observed after transition using the Q criterion. This was also the conclusion of Jimenez *et al.* (2010) from their DNS of channel and boundary layer flows, the latter reaching Re_θ up to 2,000.

The present research utilized the zero pressure gradient flat-plate boundary layer DNS of Wu & Moin (2010). This simulation extended their earlier one to $Re_\theta = 1950$ and also had a constant temperature passive heating of the wall. Our investigation of this database had several goals. First, we wanted to show that turbulence in its embryonic state in the form of turbulent spots during transition at low Reynolds numbers is quite like turbulence in its developed state at higher Reynolds numbers, both statistically and with regard to its structure. To study the statistical similarity, we compared distributions of various properties, including those of both the velocity and the velocity gradient fields, at $Re_\theta = 1850$, where the turbulence is well developed, to the property distributions at $Re_\theta = 500$, where the turbulent spots have just merged. Second, we wanted to see if the hairpin vortex structures readily seen at low Reynolds numbers in the transitional flow could be identified with vorticity lines and also if the same method could be used to identify hairpin vortices in the developed turbulence at higher Reynolds numbers. Third and finally, we wanted to study the relationship of heat and momentum transport processes to the hairpin vortices with the aim of eventually developing simple models.

2. Statistical comparison of transitional and developed turbulence

In order to compare statistical properties of the turbulence at $Re_\theta = 500$ with those at $Re_\theta = 1850$, time steps in the database where the turbulent spots have merged so that they span the computational domain for the low Reynolds number case were identified. Thirteen files were selected, an example of which is shown in Fig. 1(b). Statistics of the turbulence velocity and velocity gradient field properties, excluding any non-turbulent data, for the $Re_\theta = 500$ case were obtained by averaging the instantaneous streamwise (x) and wall normal (y) velocity components for the thirteen selected files over planes at constant y , which spanned the domain in the z direction and were $0.03Re_\theta$ wide in the x direction. Even though this flow is weakly inhomogeneous in the streamwise direction, averaging over planes that are narrow in this direction was judged appropriate. The flow is

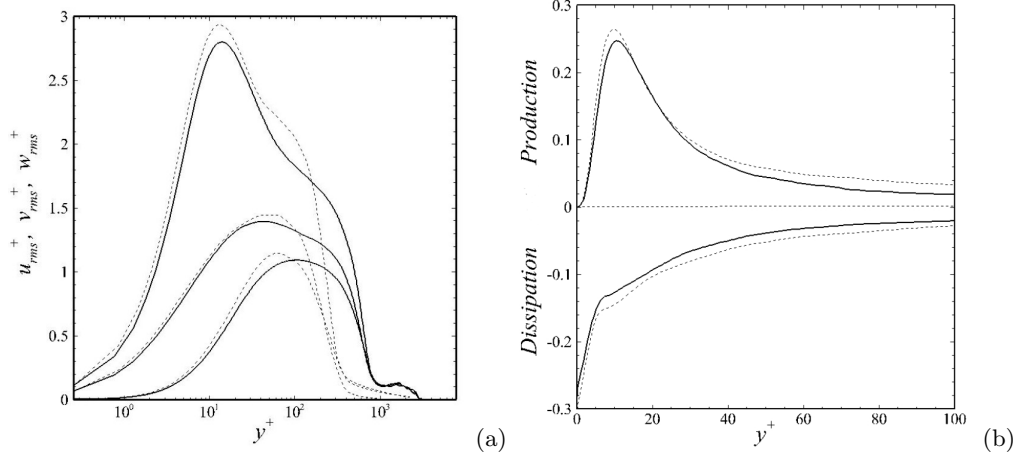


FIGURE 3. (a) Distributions of u_{rms} (top), w_{rms} (middle) and v_{rms} (bottom). (b) Distributions of the turbulent kinetic energy production and dissipation rates. Solid, $Re_\theta = 1850$; dashed, $Re_\theta = 500$.

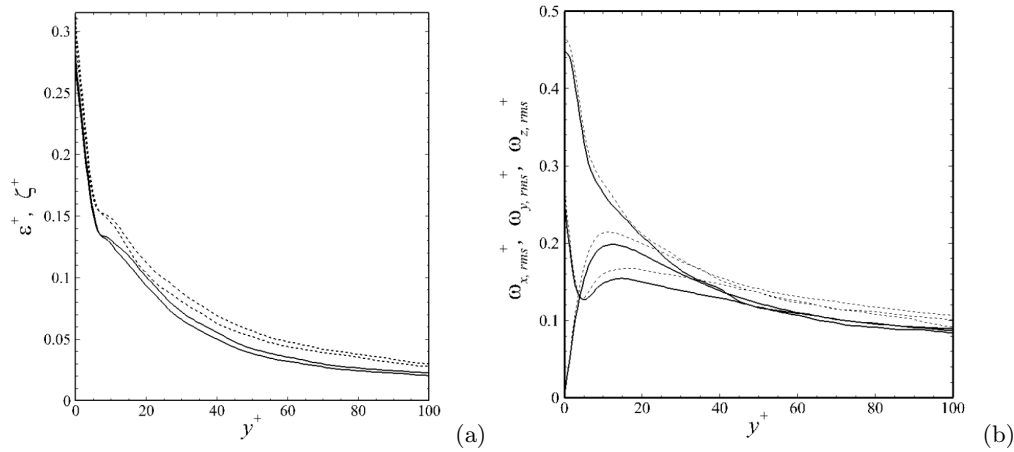


FIGURE 4. (a) Distributions of the dissipation rate and enstrophy. Upper curves are dissipation rate; lower curves are enstrophy for each Reynolds number. (b) Distributions of the rms vorticity components. At $y^+ = 0$, component curves, z : upper, x : middle, y : lower. Solid, $Re_\theta = 1850$; dashed, $Re_\theta = 500$.

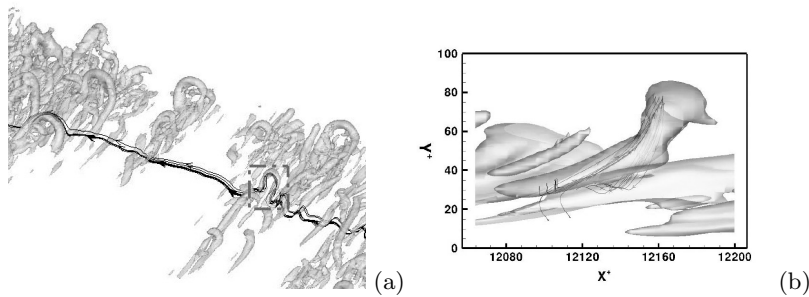


FIGURE 5. (a) Field of hairpin vortices in transitional turbulence at $Re_\theta = 500$ indicated by isosurfaces of Q . Hairpin vortex highlighted in the field is also indicated by vorticity lines initiated in its head. (b) View in spanwise direction of the highlighted hairpin.

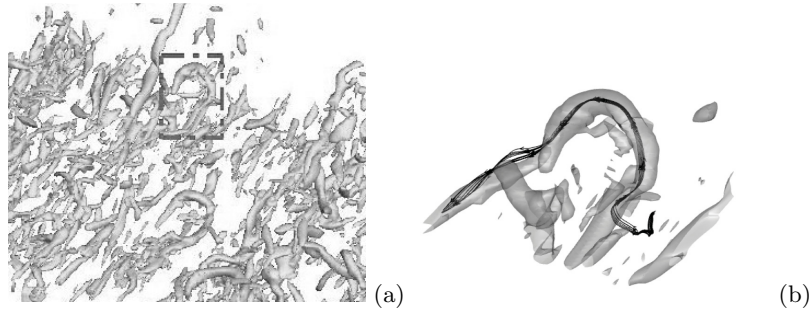


FIGURE 6. (a) Hairpin vortex in developed turbulence at $Re_\theta = 1850$ indicated by isosurfaces of Q . (b) Closeup of highlighted hairpin with vorticity lines superimposed.

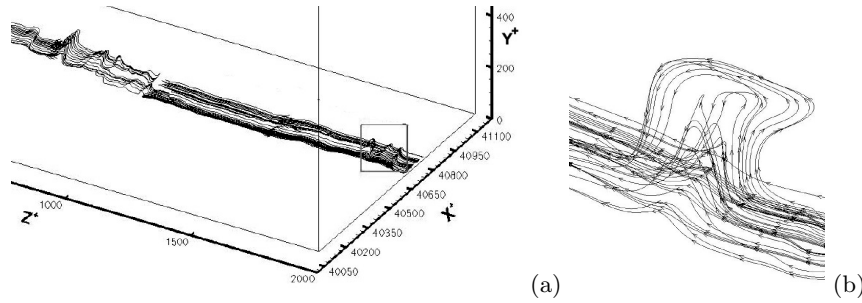


FIGURE 7. (a) Emerging hairpin vortices in developed turbulence at $Re_\theta = 1850$ indicated by vorticity lines initiated just above the sublayer. (b) Closeup of highlighted region.

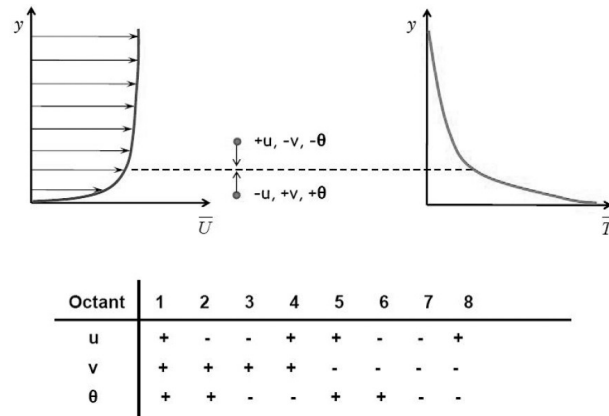


FIGURE 8. (a) Particle motions in wall normal direction illustrating momentum and heat fluxes corresponding to mean gradient transport. (b) Classification of velocity component and temperature fluctuations in octants according to their sign.

homogeneous in the spanwise direction, and the mean velocity in this direction is zero by symmetry. The mean velocity components obtained from this averaging procedure were subtracted from the instantaneous values to determine the values of the fluctuations. Velocity gradients were determined by finite difference. Normalization, indicated by the symbol $^+$, is with the friction velocity, u_τ , and the viscous length scale, ν/u_τ , where ν is the kinematic viscosity. The friction velocity for $Re_\theta = 500$ was determined from the slope at the wall of the mean streamwise velocity distribution, obtained as described

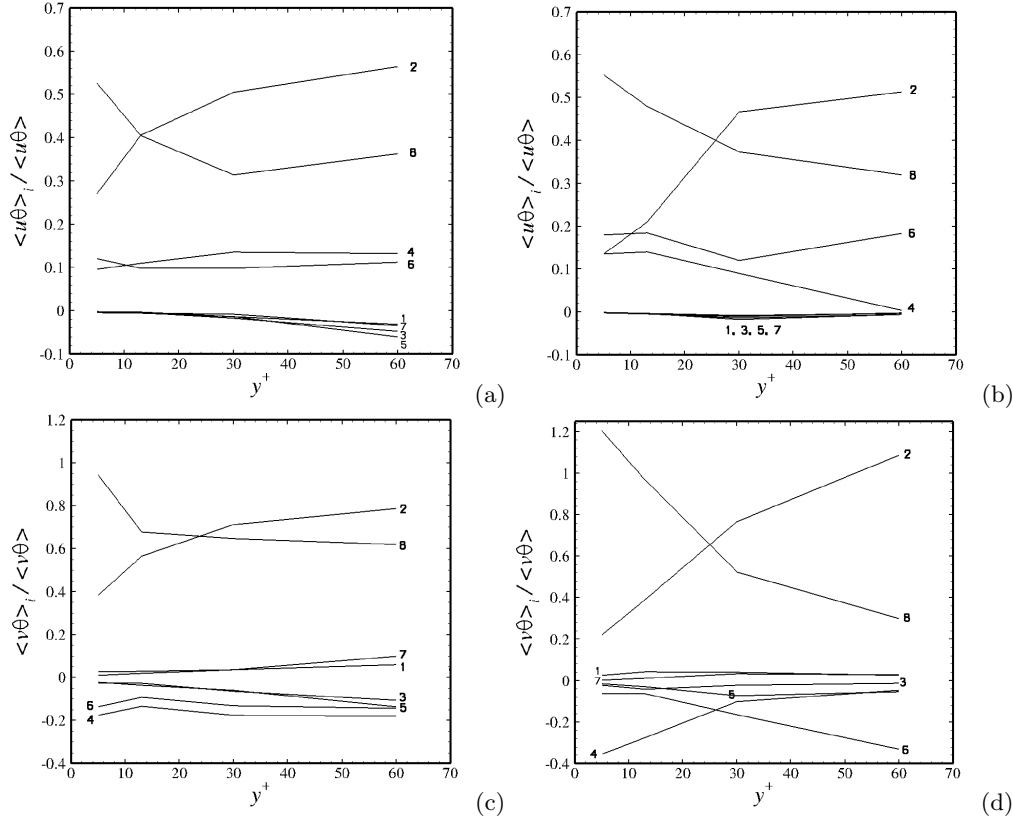


FIGURE 9. Fractional contributions to heat fluxes from the eight octants defined in figure 12. Numbers in this figure denote octants. (a) & (c) $Re_\theta = 1850$, (b) & (d) $Re_\theta = 500$.

above. The wall shear stress value corresponding to this value of u_τ that excluded non-turbulent information was normalized to give a value of the coefficient of friction, C_f . This is plotted as the circle in Fig. 2(a), which has been added to the plot of C_f versus Re_θ adapted from Wu & Moin (2010). The dotted line extrapolated backward from the turbulent region clearly shows that the low Reynolds number transitional value of C_f , obtained when only turbulent spots is averaged, comports with the values in the turbulent region where $Re_\theta > 1000$. For the developed turbulence at $Re_\theta = 1850$, the statistics were obtained in a similar manner except that there was no non-turbulent data that had to be excluded, so spanwise lines of data at $Re_\theta = 1850$ could be averaged over all the available simulation files.

In Fig. 2(b) the distribution of the mean streamwise velocity is shown. For $Re_\theta = 1850$ a logarithmic layer has formed with a Karman constant, $\kappa = 0.415$ and an intercept of 5.70 determined with a least squares fit of the data between $y^+ = 25 - 132$. For $Re_\theta = 500$ a logarithmic layer has not yet developed, a fact that has previously been observed for turbulent spots (e.g. Krishnan & Sandham 2006). The rms velocity distributions of all components are quite similar for both the developed and transitional states in the viscous and buffer layers where $y^+ < 30$, as shown in Fig. 3(a). Farther from the wall low Reynolds number effects become evident as the low Reynolds number curves rolloff at lower values of y^+ than for the higher Reynolds number developed turbulence case.

In Fig. 3(b) the normalized production and dissipation rates of turbulent kinetic energy for the transitional and developed Reynolds number cases are shown. Although both variables have a little higher values in parts of the boundary layer for the transitional case, the distributions are remarkably similar. Likewise, the comparison of the distributions of dissipation rate and enstrophy in Fig. 4 shows only small differences between the transitional and developed cases. The full dissipation rate and enstrophy are exactly related by $\epsilon = \nu[(\omega_i)^2 + 2\overline{\partial u_i/\partial x_j \partial u_j/\partial x_i}]$. Near the wall in this boundary layer they are almost identical, with the dissipation rate becoming somewhat larger than the enstrophy in the buffer layer and above. In Fig. 4 the distributions of the components of fluctuating vorticity are compared. Although there are some differences between the $Re_\theta = 500$ transitional flow and the $Re_\theta = 1850$ developed flow, with the transitional case having a little larger magnitudes, the trends for the two cases are generally quite similar.

2.1. Structure

In Fig. 5(a) a segment of the flow domain for $Re_\theta = 500$ is shown where isosurfaces of Q have been displayed and vorticity lines have been started in the “head” of the hairpin which has been highlighted. In (b) of this figure, which zooms in on the hairpin as viewed in the spanwise direction, it is apparent that the vorticity lines identify the same structure as Q . The highlighted hairpin vortex in Fig. 6(a) for $Re_\theta = 1850$ is shown in (b) of the same figure with the vorticity lines superimposed which were initiated in its head. When the threshold of Q that gave this good coincidence between the Q isosurfaces and the vorticity lines was raised or lowered, the coincidence was lost. When vorticity lines are initiated at the right side of the computational domain just above the sublayer for $Re_\theta = 1850$, they generally are oriented in the spanwise direction, indicating a sheet-like structure. However, they lift upward from the wall at several locations across the flow in the form of beginning hairpin vortices. An example is shown in Fig. 7(a), and (b) of the figure is a zoomed image of the highlighted region.

2.2. Transport Processes

When streamlines are plotted in cross-stream ($y - z$) planes cut through the legs of the hairpin vortices in both the transitional and developed flow cases, counter-rotating vortices are evident. Strong momentum and heat fluxes, which are associated with the vortices, occur in the local flows toward and away from the wall. Figure 8 illustrates wall normal motions of fluid particles, and the fluxes which they produce that are of the classical mean gradient type. Also shown in the figure is a table classifying the momentum $\langle uv \rangle$ and heat $\langle uc \rangle$ and $\langle vc \rangle$, fluxes according to the sign of the fluctuations of the velocity components and temperature about their respective mean values. It is apparent that the two types of particle motions shown in the figure that comport with mean gradient transport are those in octants 2 and 8. All the other octants correspond to counter-mean gradient type fluxes. Because mean-gradient transport is relative simple to model, it is of real interest to determine where in a particular flow, if at all, is this type of transport dominant. We calculated the fractional contributions to the $\langle u\theta \rangle$ and $\langle v\theta \rangle$ heat fluxes from each octant category for this boundary layer. The distributions are shown in Fig. 9, where it is seen that the mean gradient transport octants, 2 and 8, are indeed dominant throughout much of the flow.

3. Conclusions

This investigation of turbulent states in transition at $Re_\theta = 500$, where individual turbulent spots have merged, and at $Re_\theta = 1850$, where the turbulence is developed, revealed the following:

1. The statistics obtained from the fluctuating velocity and the velocity gradient tensor components are quite similar for the two cases provided only time instances when the flow is turbulent are used to determine the statistics for the transitional case.

2. Vorticity lines successfully identified hairpin vortices in both flow states that had also been identified with isosurfaces of the second invariant of the velocity gradient tensor, Q . Whether or not the Q criterion identified a particular vortex depended on the threshold level used, which is not the case for the vorticity lines. However, the starting location of the vorticity line integration had to be judiciously chosen for the vortex to be identified.

3. Bundles of beginning hairpin-shaped vorticity lines frequently lift up out of sheets of spanwise vorticity very near the wall.

4. Throughout much of the boundary layer, the motions contributing to the heat fluxes, $\langle u\theta \rangle$ and $\langle v\theta \rangle$, are dominantly of the mean gradient type, as shown by an octant analysis of the flow based on the signs of the fluctuations, u , v and θ . This transport is closely associated with the presence of the hairpin vortices in this flow. The octant analysis was applied to both the transitional and developed turbulence data, with similar results for both cases.

In summary, the comparison of the turbulence in transition with that in the developed flow shows that the two states are very similar. This is strong evidence that the structure and transport processes of a developed turbulent boundary layer is little different from those in its embryonic form in transitional turbulent spots.

JMW and XW gratefully acknowledge support from the CTR 2010 Summer Program.

REFERENCES

- ADRIAN, R. J. 2007 Hair-pin vortex organization in wall turbulence. *Phys. Fluids* **19**, 041301.
- BALINT, J.-L., WALLACE, J. M. & VUKOSLAVČEVIĆ, P. 1992 The velocity and vorticity fields in a turbulent boundary layer. Part 2. Statistical properties. *J. Fluid Mech.* **189**, 53–86.
- CANTWELL, B., COLES, D. & DIMOTAKIS, P. 1978 Structure and entrainment in the plane of symmetry of a turbulent spot. *J. Fluid Mech.* **87**, 641–672.
- CORINO, E. R. & BRODKEY, R. S. 1969 A visual investigation of the wall region in turbulent flow. *J. Fluid Mech.* **37**, 1–30.
- EMMONS, H. W. 1951 The laminar-turbulent transition in a boundary layer. Part 1. *J. Aero. Sci.* **18**, 490–498.
- HENNINGSON, D. S., SPALART, P. & KIM, J. 1987 Numerical simulations of turbulent spots in plane Poiseuille and boundary layer flows. *Phys. Fluids* **30**, 2914–2917.
- HENNINGSON, D. S. & KIM, J. 1991 On turbulent spots in plane Poiseuille flow. *J. Fluid Mech.* **228**, 183–205.
- JACOBS, R. G. & DURBIN, P. A. 2001 Simulations of bypass transition. *J. Fluid Mech.* **428**, 185–212.
- JIMENEZ, J., HOYAS, S., SIMENS, M. & MIZUNO, Y. 2010 Turbulent boundary layers and channels at moderate Reynolds numbers. *J. Fluid Mech.* **657**, 335–360.

- KATZ, Y., SIEFERT, A. & WYGNANSKI, I. 1990 On the evolution of the turbulent spot in a laminar boundary layer with a favorable pressure gradient. *J. Fluid Mech.* **221**, 1–22.
- KIM, J. & MOIN, P. 1986 The structure of the vorticity field in turbulent channel flow: Part 2. Study of ensemble-averaged fields. *J. Fluid Mech.* **162**, 339–363.
- KLEBANOFF, P. S. 1954 Characteristics of turbulence in a boundary layer with zero pressure gradient. *NACA TN* **3178**.
- KLINE, S. J., REYNOLDS, W. C., SCHRAUB, F. A. & RUNDSTADLER, P. W. 1967 The structure of turbulent boundary layers. *J. Fluid Mech.* **30**, 741–743.
- KRISHNAN, L. & SANDHAM, N.D. 2006 On the merging of turbulent spots in a supersonic boundary-layer flow. *Int. J. of Heat and Fluid Flow*. **27**, 542–550.
- MOIN, P. & KIM, J. 1985 The structure of the vorticity field in turbulent channel flow: Analysis of instantaneous fields and statistical correlations. *J. Fluid Mech.* **155**, 441–464.
- PRANDTL, L. 1904 Über flüssigkeit bei sehr kleiner reibung. *Proc. 3rd Int. Math. Congr.*, Heidelberg.
- PURTELL, L. P., KLEBANOFF, P. S. & BUCKLEY, F. T. 1981 Turbulent boundary layer at low Reynolds number. *Phys. Fluids* **24**, 802–811.
- ROBINSON, S. K. 1991 Coherent motion in the turbulent boundary layer. *Ann. Rev. Fluid Mech.* **23**, 601–639.
- SCHLATTER, P., QUIANG, L., BRETHOUWER, G., JOHANNSON, A. V. & HENNINGSON, D. S. 2010 Simulations of spatially evolving turbulent boundary layers up to $Re_\theta = 4300$. *Int. J. of Heat and Fluid Flow* **31**, 251–261.
- SINGER, B. A. 1996 Characteristics of a young turbulent spot. *Phys. Fluids* **8**, 509–521.
- SINGER, B. A. & JOSLIN, R. D. 1994 Metamorphosis of a hairpin vortex into a young turbulent spot. *Phys. Fluids* **6**, 3724–3736.
- SPALART, P. 1988 Direct simulation of a turbulent boundary layer up to $Re_\theta = 1410$. *J. Fluid Mech.* **187**, 61–98.
- THEODORSEN, T. 1952 Mechanism of turbulence. *Proc. Midwestern Conf. Fluid Mech.* Ohio State Univ., Columbus, OH.
- WALLACE, J. M., BRODKEY, R. S. & ECKELMANN, H. 1972 The wall region in turbulent shear flow. *J. Fluid Mech.* **54**, 39–48.
- WALLACE, J. M. 1982 On the structure of bounded turbulent shear flow: A personal view. in *Devel. in Theoret. & Appl. Mech.* **XI**, (ed. T.J. Chung and G.R. Karr), Univ. of Alabama at Huntsville, 509–521.
- WALLACE, J. M. 1985 The vortical structure of bounded turbulent shear flow. *Lect. Notes in Phys.* **235**, Flow of Real Fluids (eds. G. Meier and F. Obermeier), 253–268.
- WILLMARTH, W. W. 1975 Structure of turbulence in boundary layers. *Adv. in Appl. Mech.* **15**, Academic Press, 159–254.
- WYGNANSKI, I., HARITONIDIS, J. H. & KAPLAN, R. E. 1979 On a Tollmien-Schlichting wave packet produced by a turbulent spot. *J. Fluid Mech.* **92**, 505–528.
- WU, X. & MOIN, P. 2009 Direct numerical simulation of turbulence in a nominally zero-pressure-gradient flat-plate boundary layer. *J. Fluid Mech.* **630**, 5–41.
- WU, X. & MOIN, P. 2010 Transitional and turbulent boundary layer with heat transfer. *Phys. Fluids* **22**, 085105.